B_c mesons and their properties on the light front

Shuo Tang,[1,*] Yang Li,[2] Pieter Maris,[1] and James P. Vary[1]
[1]Department of Physics and Astronomy, Iowa State University, Ames, Iowa 50011, USA
[2]Department of Physics, College of William & Mary, Williamsburg, Virginia 23185, USA

(Received 25 October 2018; published 28 December 2018)

We investigate the unequal-mass relativistic bound-state system, the B_c mesons, in a light-front Hamiltonian formalism. We adopt an effective Hamiltonian based on soft-wall light-front holography, together with a longitudinal confinement that was first introduced for heavy quarkonium. We also include the one-gluon-exchange interaction with a running coupling, which produces the spin structure. We present the mass spectrum and light-front wave functions. We also use the light-front wave functions to calculate decay constants, charge and momentum densities, as well as distribution amplitudes. The results are compared with experiments and other theoretical approaches, all of which are in reasonable agreement.

DOI: 10.1103/PhysRevD.98.114038

I. INTRODUCTION

The B_c system is the only known heavy meson family with unequal quark masses, which provides an important testing ground for understanding strong interaction physics. While the spectra and properties of the $c\bar{c}$ and $b\bar{b}$ mesons are extensively studied in experiments, data on $b\bar{c}$ or $c\bar{b}$ are relatively scarce. Until now, only two states, the ground state and its first radial excitation, have been confirmed in experiments [1,2]. Meanwhile, ongoing and forthcoming high energy experiments, e.g., the LHC and Relativistic Heavy Ion Collider, are expected to generate a large ensemble of these particles. For these reasons, there are renewed interests in theoretical investigations [3–6].

Light-front quantization is a natural relativistic framework to describe the intrinsic partonic structure of hadrons [7]. Among various light-front approaches, light-front holographic (LFH) models stand out as semiclassical approximations to QCD (see Ref. [8] and the references therein). Meanwhile, a computational framework known as the basis light-front quantization (BLFQ), has been established to tackle the many-body dynamics and has been applied to QED [9,10] and QCD [11,12] bound states. In the latter case, LFH is embedded in the BLFQ formulation to model the heavy quarkonium (charmonium and bottomonium) system. The results have shown good agreement with experiments and other theoretical models.

In this work, we adapt the successful Hamiltonian of Refs. [11,12] to the B_c system in the BLFQ approach. In essence, this model implements the AdS/QCD soft-wall Hamiltonian [13] plus a longitudinal confinement [11], both of which are of long range. In addition, we adopt the one-gluon exchange with a running coupling [12]. This term controls the short-distance physics and embeds the spin structure information. We solve the B_c system without introducing any additional free parameter (other than the ones employed in charmonium and bottomonium). Therefore, it is also a test of the predictive power of the model proposed in Ref. [12]. This work is a straightforward yet necessary step for developing a relativistic model for hadrons based on light-front holography and light-front dynamics.

We begin by introducing the effective light-front Hamiltonian and the basis function approach in Sec. II, following Ref. [12]. Presented in Sec. III are results including the mass spectrum, wave functions, decay constants, transverse charge and momentum density, and distribution amplitudes. They are compared with experiments and other theories whenever available. We also discuss the differences between B_c and heavy quarkonium. Section IV summarizes our current work and provides a brief discussion of possible improvements.

II. HAMILTONIAN FORMALISM AND THE BASIS FUNCTION REPRESENTATION

The light-front Hamiltonian formalism leads to an eigenvalue equation $H|\psi_h\rangle = M_h^2|\psi_h\rangle$. Here, we adapt the effective Hamiltonian of Refs. [11–13] for unequal quark masses,

$$H_{\rm eff} = \frac{\vec{k}_\perp^2 + m_q^2}{x} + \frac{\vec{k}_\perp^2 + m_{\bar{q}}^2}{1-x} + \kappa^4 \vec{\zeta}_\perp^2 - \frac{\kappa^4}{(m_q + m_{\bar{q}})^2}\partial_x(x(1-x)\partial_x) - \frac{C_F 4\pi\alpha_s(Q^2)}{Q^2}\bar{u}_{s'}(k')\gamma_\mu u_s(k)\bar{v}_{\bar{s}}(\bar{k})\gamma^\mu v_{\bar{s}'}(\bar{k}'), \quad (1)$$

*tang@iastate.edu

TABLE I. Summary of the model parameters.

	N_f	κ (GeV)	m_c (GeV)	m_b (GeV)	r.m.s (MeV)	$\overline{\delta_j M}$ (MeV)	$N_{\max} = L_{\max}$	Ref.
$c\bar{c}$	4	0.966	1.603	⋯	31	17	32	[12]
$b\bar{b}$	5	1.389	⋯	4.902	38	8	32	[12]
$b\bar{c}$	4	1.196	1.603	4.902	37	6	32	This work

where $\vec{\zeta}_\perp \equiv \sqrt{x(1-x)}\vec{r}_\perp$ is the holographic variable [8] and $C_F = (N_c^2 - 1)/(2N_c) = 4/3$ is the color factor of the $q\bar{q}$ color singlet state. In this paper, we investigate the B_c system as $b\bar{c}$, i.e., B_c^-. Therefore, m_q is the mass of the bottom quark, and $m_{\bar{q}}$ the anticharm quark. x and $(1-x)$ are the longitudinal momentum fractions of b and $\bar{c}$, respectively. We incorporate a running coupling for the one-gluon-exchange potential, which is modeled as [12]

$$\alpha_s(Q^2) = 1/[\beta_0 \ln(Q^2/\Lambda^2 + \tau)], \tag{2}$$

where $\beta_0 = (33 - 2N_f)/(12\pi)$, with the quark flavor number taken to be $N_f = 4$. We use $\Lambda = 0.13$ GeV, and in order to avoid the perturbative QCD IR divergence, we use $\tau = 12.3$ such that $\alpha(0) = 0.6$. See Ref. [12] for more details.

We adopt a Fock space limited to the $|q\bar{q}\rangle$ sector where the state vector reads

$$\begin{aligned}|\psi_h(P,j,m_j)\rangle = \sum_{s,\bar{s}} \int_0^1 \frac{\mathrm{d}x}{2x(1-x)} \int \frac{\mathrm{d}^2k_\perp}{(2\pi)^3} \psi^{(m_j)}_{s\bar{s}/h}(\vec{k}_\perp, x) \\ \times \frac{1}{\sqrt{N_c}} \sum_{i=1}^{N_c} b^\dagger_{si/b}(xP^+, \vec{k}_\perp + x\vec{P}_\perp) \\ \times d^\dagger_{\bar{s}i/\bar{c}}((1-x)P^+, -\vec{k}_\perp + (1-x)\vec{P}_\perp)|0\rangle.\end{aligned} \tag{3}$$

In the expression above, $\psi^{(m_j)}_{s\bar{s}/h}(\vec{k}_\perp, x)$ represents the light-front wave functions (LFWFs), and s and $\bar{s}$ are the spins of the quark and antiquark, respectively. The anticommutation relations of creation operators and the orthonormal relation of state vectors in this work are similar to those for heavy quarkonium [12].

We use a basis function approach, BLFQ [14], and following Ref. [11], we represent the LFWFs in terms of transverse and longitudinal basis functions ϕ_{nm} and χ_l, with basis coefficients $\psi_h(n,m,l,s,\bar{s})$,

$$\psi^{(m_j)}_{s\bar{s}/h}(\vec{k}_\perp, x) = \sum_{n,m,l} \psi_h(n,m,l,s,\bar{s}) \phi_{nm}(\vec{k}_\perp/\sqrt{x(1-x)}) \chi_l(x). \tag{4}$$

For the basis functions, we employ

$$\begin{aligned}\phi_{nm}(\vec{q}_\perp; b) &= \frac{1}{b}\sqrt{\frac{4\pi n!}{(n+|m|)!}}\left(\frac{q_\perp}{b}\right)^{|m|} \\ &\quad \times e^{-\frac{1}{2}q_\perp^2/b^2} L_n^{|m|}(q_\perp^2/b^2) e^{\mathrm{i}m\theta_q}, \\ \chi_l(x;\alpha,\beta) &= \sqrt{4\pi(2l+\alpha+\beta+1)} \\ &\quad \times \sqrt{\frac{\Gamma(l+1)\Gamma(l+\alpha+\beta+1)}{\Gamma(l+\alpha+1)\Gamma(l+\beta+1)}} \\ &\quad \times x^{\frac{\beta}{2}}(1-x)^{\frac{\alpha}{2}} P_l^{(\alpha,\beta)}(2x-1),\end{aligned} \tag{5}$$

which are the analytical solutions of the effective Hamiltonian without the one-gluon exchange. Here, ϕ_{nm} is the two-dimensional harmonic oscillator function with n and m the principle and orbital angular momentum quantum numbers, respectively, with $\vec{q}_\perp = \vec{k}_\perp/\sqrt{x(1-x)}$, $q_\perp = |\vec{q}_\perp|$, $\theta_q = \arg \vec{q}_\perp$, and $L_n^{|m|}(z)$ is the associated Laguerre polynomial. Note that the conserved total magnetic projection m_j is the sum of the orbital projection m and the sum of the spin projections, $m_j = m + s + \bar{s}$. We adopt $b = \kappa$ for the scale parameter in the harmonic oscillator basis. For the longitudinal basis function χ_l, l is the longitudinal quantum number, and $P_l^{(\alpha,\beta)}(z)$ is the Jacobi polynomial. The dimensionless parameters α and β are associated with the quark masses: $\alpha = 2m_{\bar{c}}(m_b + m_{\bar{c}})/\kappa^2$ and $\beta = 2m_b(m_b + m_{\bar{c}})/\kappa^2$. When the one-gluon exchange is implemented, one can solve the eigenequation by diagonalizing the Hamiltonian matrix. Hence, the obtained eigenvalues represent the spectra as squared masses, and the eigenvectors are the coefficients $\psi_h(n,m,l,s,\bar{s})$.

III. NUMERICAL RESULTS

In this work, we adopt model parameters from those of the charmonium and bottomonium calculations without doing further parameter fitting. In particular, we adopt the quark masses from the charmonium and bottomonium applications [12] (see Table I). On the other hand, the confining strength is taken as $\kappa_{b\bar{c}} = \sqrt{(\kappa_{c\bar{c}}^2 + \kappa_{b\bar{b}}^2)/2}$, where $\kappa_{b\bar{b}}$ and $\kappa_{c\bar{c}}$ are the confining strength of the charmonium and bottomonium system, respectively. This is in accordance with the heavy quark effective theory [15]. All the calculations in this paper, unless otherwise stated, are based on $N_{\max} = L_{\max} = 32$, which is associated with UV and IR

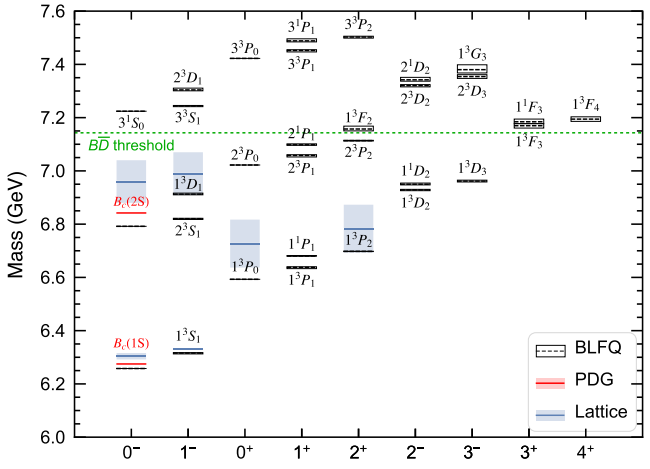

FIG. 1. The reconstructed $B_c(b\bar{c})$ spectrum at $N_{\max} = L_{\max} = 32$. The horizontal axis is J^{P}, and the vertical axis is invariant mass in giga-electron-volts. We compare with data from PDG [16] and Lattice [17–19], with central values shown as solid lines and uncertainties as shades.

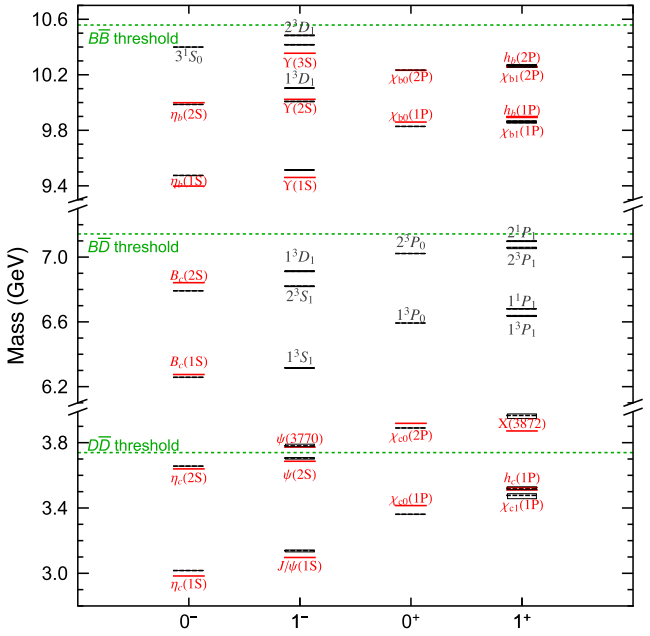

FIG. 2. The mass spectrum for charmonium, B_c, and bottomonium below their respective dissociation thresholds. Note that, aside from an overall shift, the mass scales are similar. We only select the states with $J = 0$ and 1 for comparison. Experimental results from PDG [16] are in red, while our results are in black. The spread in m_j values, defined in Eq. (7), is indicated by a rectangular black box around the $J = 1$ theory results. This is scarcely visible in many cases. The mean spread of charmonium is larger than the other two. All the three systems have similar patterns in the spectrum, while the heavier system has more states below the threshold.

regulators $\Lambda_{\rm UV} = b\sqrt{N_{\max}} \simeq 6.77$ GeV and $\lambda_{\rm IR} = b/\sqrt{N_{\max}} \simeq 0.21$ GeV.

A. Mass spectroscopy

In order to identify the multiplet of magnetic substates belonging to a single angular momentum j, the effective Hamiltonian is diagonalized for various m_j's. One needs to perform the state identification to deduce the full set of quantum numbers $\mathsf{n}^{2s+1}\ell_j$ or j^{P}, where ℓ is the orbital angular momentum and n is the radial quantum number (not to be confused with the basis quantum numbers n and l). The reconstructed mass spectrum up to the $B\bar{D}$ open flavor threshold is presented in Fig. 1, in which we use the dashed lines for the mean values of invariant masses:

$$\overline{M} \equiv \sqrt{\frac{M_{-j}^2 + M_{1-j}^2 + \cdots + M_j^2}{2j+1}}. \tag{6}$$

The boxes indicate the spread from different m_j, i.e., $\delta_j M \equiv \max(M_{m_j}) - \min(M_{m_j})$, which is nonzero due to the violation of rotational symmetry arising from the Fock space and basis space truncations. We also employ the mean spread to quantify the rotational symmetry violation from all high spin states below their respective dissociation thresholds,

$$\overline{\delta_j M} \equiv \sqrt{\frac{1}{N_h}\sum_h^{j\neq 0}(\delta_j M_h)^2} \quad \left(N_h \equiv \sum_h^{j\neq 0} 1\right). \tag{7}$$

We provide the experimental values compiled by the Particle Data Group (PDG) [16] and results from Lattice [17–19] for comparison. Note that the rms deviations in Table I are evaluated with respect to 8 and 14 states for charmonium and bottomonium [12], but only with respect to two experimental states for B_c.

We note that the mean spread of $b\bar{c}$, which is evaluated with a total of 12 states below the threshold of this system, is smallest in Table I. We compare the mass spectrum of B_c and heavy quarkonia in Fig. 2 for selected states. It is a challenge to visually ascertain which system exhibits the best rotational symmetry. However, as evident from Table I, on the basis of the fraction of the mean spread relative to the total mass, we can see that the violation of rotational symmetry is larger for charmonium than for B_c and bottomonium. This suggests heavier systems retain rotational symmetry in our approach better than lighter systems.

B. Light-front wave functions

Obtaining the LFWFs is a major motivation for this formalism, as they provide direct access to hadron observables. We present some of the valence LFWFs with different polarization and spin alignments for B_c states. Specifically, we have the relation $m_j = s_1 + s_2 + m$, where m is the orbital angular momentum projection. Since the phase

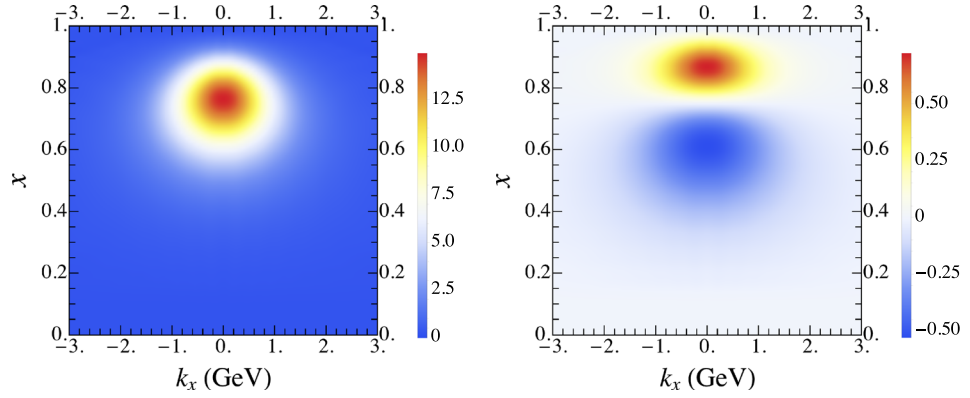

a) $\psi_{\uparrow\downarrow-\downarrow\uparrow}(k_x, k_y = 0, x)$. **Left** : $(m + l) =$ Even; **Right** : $(m + l) =$ Odd.

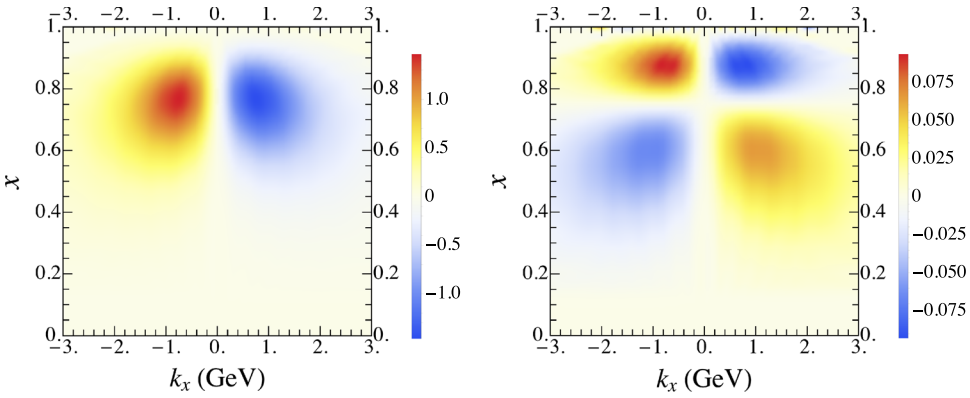

b) $\psi_{\downarrow\downarrow}(k_x, k_y = 0, x) = \psi^*_{\uparrow\uparrow}(k_x, k_y = 0, x)$. **Left** : $(m + l) =$ Even; **Right** : $(m + l) =$ Odd.

FIG. 3. LFWFs of the ground state B_c shown as plots of their magnitudes vs x and k_x at $k_y = 0$. In general, spin alignment a) is dominant and reminiscent of nonrelativistic behavior, while b) is purely a relativistic component.

$\exp(im\theta)$ factorizes in the wave function on the two-body level, we drop it while retaining the sign for negative $\vec{k}_\perp$; i.e., we visualize the LFWFs at $k_y = 0$ ($\theta = 0$ and $\theta = \pi$).

In Fig. 3, we show the ground state pseudoscalar LFWFs. There are two independent components with different spin alignments for the 0^- state: $\psi_{\uparrow\downarrow-\downarrow\uparrow}(\vec{k}_\perp, x) \equiv \frac{1}{\sqrt{2}}[\psi_{\uparrow\downarrow}(\vec{k}_\perp, x) - \psi_{\downarrow\uparrow}(\vec{k}_\perp, x)]$ and $\psi_{\downarrow\downarrow}(\vec{k}_\perp, x) = \psi^*_{\uparrow\uparrow}(\vec{k}_\perp, x)$. The former is dominant and reduces to the nonrelativistic wave function in the heavy quark limit, while the latter is of pure relativistic origin.

Furthermore, B_c has another significant feature that is distinguished from quarkonium (the equal-mass mesons). For the heavy quarkonia, charge conjugation is a good symmetry and is reflected by states having components either even or odd in $(m + l)$ [11]. There is no charge conjugation symmetry of B_c, but we do observe that our solutions are dominated by either even or odd $(m + l)$. Table II exhibits this dominance, along with the comparison with heavy quarkonia of the ground states. In a separate test calculation, we verified that, as the mass difference between quark and antiquark decreases, the contribution from even $(m + l)$ is getting smaller and progresses smoothly to the equal-mass limit.

The LFWFs of B_c do not have symmetry with respect to $x = \frac{1}{2}$ in the longitudinal direction, another feature distinguishing B_c from heavy quarkonium. The wave function peaks in x near the bottom quark mass fraction, i.e., $x = m_b/(m_b + m_{\bar{c}}) \approx 0.75$, as expected from the major role of the kinetic energy terms in the Hamiltonian. This asymmetry will have interesting consequences for other observables as discussed in the following subsections.

TABLE II. The probabilities of finding the specified even or odd $(m + l)$ in the ground state of heavy mesons. The dominant spin alignment listed here is the components that persist in the nonrelativistic limit. Note the systematic increase of these dominant components with the increasing meson mass.

	Even/odd $(m + l)$			
	$\lvert\psi_{\uparrow\downarrow-\downarrow\uparrow}(\vec{k}_\perp, x)\rvert^2$		$\lvert\psi_{\downarrow\downarrow}(\vec{k}_\perp, x)\rvert^2 + \lvert\psi_{\uparrow\uparrow}(\vec{k}_\perp, x)\rvert^2$	
System	Odd	Even	Odd	Even
$c\bar{c}$	88.01%	0	11.99%	0
$b\bar{c}$	91.62%	0.35%	7.98%	0.05%
$b\bar{b}$	96.61%	0	3.39%	0

TABLE III. Pseudoscalar and vector decay constants of the ground state B_c and its vector partner B_c^*. The uncertainties of this work indicate the sensitivity to basis truncation, which is taken to be $\Delta f_{b\bar{c}} = 2|f_{b\bar{c}}(N_{\max} = 32) - f_{b\bar{c}}(N_{\max} = 24)|$. The results (this work) are compared with those from lattice QCD (Lattice, [3,4]), QCD sum rules [21,22], light-front quark model (LFQM, [23]), covariant confined quark model (CCQM, [24]) and Bethe-Salpeter equations (BSE, [26]). An early effort using QCD sum rules provided 300 MeV as an estimate for f_{B_c} and 500 MeV for $f_{B_c^*}$ [28,29].

Constant (MeV)	This work	Lattice [3,4]	QCD sum rules [21,22]	LFQM [23]	CCQM [24]	BSE [26]
f_{B_c}	523(62)	427(6)	528(19)	551	489.3	578
$f_{B_c^*}$	474(42)	422(13)	384(32)	508	⋯	⋯

C. Decay constants

Meson decay constants, f_h, are hadronic properties defined from the matrix element of the local current that annihilates the meson. They are

$$\langle 0|\bar{c}\gamma^\mu\gamma_5 b|P(p)\rangle = \mathrm{i}p^\mu f_P,$$
$$\langle 0|\bar{c}\gamma^\mu b|V(p,\lambda)\rangle = e_\lambda^\mu M_V f_V, \tag{8}$$

for pseudoscalar (P) and vector (V) states, respectively. Here, p is the momentum of the meson, and e_λ^μ is the polarization vector,

$$e_\lambda^\mu(k) = (e_\lambda^-(k), e_\lambda^+(k), \vec{e}_{\perp\lambda}(k)) \triangleq \begin{cases} \left(\frac{\vec{k}_\perp^2 - M_V^2}{M_V k^+}, \frac{k^+}{M_V}, \frac{\vec{k}_\perp}{M_V}\right), & \lambda = 0 \\ \left(\frac{2\vec{e}_{\perp\lambda}\cdot\vec{k}_\perp}{k^+}, 0, \vec{e}_{\perp\lambda}\right), & \lambda = \pm 1 \end{cases}, \tag{9}$$

where $\vec{e}_{\perp\pm} = (1, \pm\mathrm{i})/\sqrt{2}$, and we adopt $\lambda \equiv m_j$ as the angular momentum projection. The decay constant can be computed in the light-front representation in terms of LFWFs with different polarizations and corresponding current components. In this work, we choose the "good current" ($\mu = +$) and the longitudinal polarization ($\lambda = 0$) for the calculations [20]. This choice leads to the decay constant as

$$\frac{f_{P,V}}{2\sqrt{2N_c}} = \int_0^1 \frac{\mathrm{d}x}{2\sqrt{x(1-x)}} \int \frac{\mathrm{d}^2k_\perp}{(2\pi)^3} \psi^{(\lambda=0)}_{\uparrow\downarrow\mp\downarrow\uparrow}(\vec{k}_\perp, x), \tag{10}$$

where the minus and plus signs correspond to the pseudoscalar and vector states, respectively. Here, calculations have been done with $N_{\max} = 32$, corresponding to $\Lambda_{\mathrm{UV}} \triangleq \kappa\sqrt{N_{\max}} \approx m_b + m_{\bar{c}}$, where Λ_{UV} is the ultraviolet regulator. This is to balance the needs for better basis resolution and a lower UV scale owing to the omitted radiative corrections. We present a survey of recent work in Table III along with results from Lattice [3,4] and other approaches (see Refs. [21–26]) for comparison. Lattice results are systematically smaller than the other methods by about 20%, as also discussed in other references (e.g., Refs. [21,27]).

In Fig. 4, we compare the vector decay constants of B_c and heavy quarkonia [12]. We can see a trend that decay constants within each meson system decrease with increasing radial quantum numbers. This trend seems reasonable since increasing radial quantum numbers correspond to less binding and a larger spread in the radial probability distributions. In addition, we note that the vector decay constants increase with the mass of the system for corresponding states, e.g., $J/\Psi < B_c(1^3S_1) < \Upsilon$. This trend correlates with decreasing size as the mass increases, which is discussed further in the next session.

D. Charge and longitudinal momentum densities

The transverse density offers insight into the hadron structure. In this work, we study the charge density in the transverse impact parameter space of B_c mesons. By definition, it is the two-dimensional Fourier transform of the Dirac form factor [30,31],

$$\rho_c(\vec{b}_\perp) = \int \frac{\mathrm{d}^2\Delta_\perp}{(2\pi)^2} e^{\mathrm{i}\vec{\Delta}_\perp\cdot\vec{b}_\perp} F_1(q^2 = -\vec{\Delta}_\perp^2), \tag{11}$$

where $\vec{\Delta}_\perp$ is the transverse momentum transfer and $\vec{b}_\perp$ can be interpreted as the conjugated position of $\vec{\Delta}_\perp$ at which the current probes the charge density. Analogous to the charge

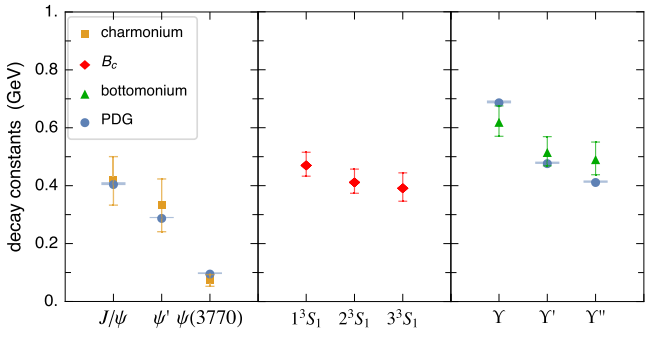

FIG. 4. The decay constants for vector states of charmonium, B_c, and bottomonium. Results of charmonium and bottomonium are from previous work [12] and the PDG [16].

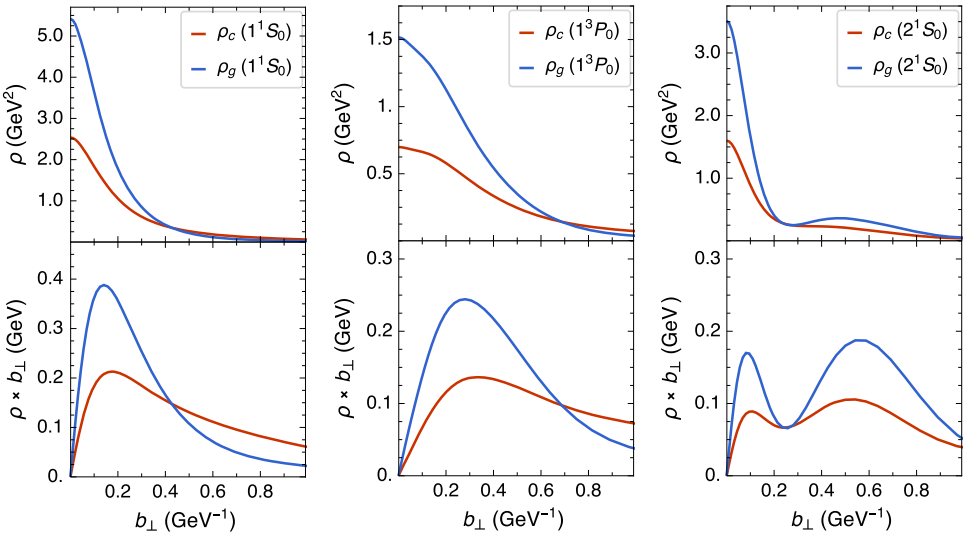

FIG. 5. The charge density and longitudinal momentum density on the transverse plane of the pseudoscalar and scalar states.

distribution, we can perform the two-dimensional Fourier transform of the gravitational form factor, which can be interpreted as the longitudinal momentum density in the transverse plane [32]. In the LFWF representation of the two-body ($b\bar{c}$) approximation, they can be expressed as

$$\rho_c(\vec{b}_\perp) = \frac{1}{3}\sum_{s,\bar{s}}\int_0^1 \frac{\mathrm{d}x}{4\pi(1-x)^2}\left|\tilde{\psi}_{s\bar{s}}\left(\frac{-\vec{b}_\perp}{1-x},x\right)\right|^2 + \frac{2}{3}\sum_{s,\bar{s}}\int_0^1 \frac{\mathrm{d}x}{4\pi x^2}\left|\tilde{\psi}_{s\bar{s}}\left(\frac{\vec{b}_\perp}{x},x\right)\right|^2, \tag{12}$$

$$\rho_g(\vec{b}_\perp) = \sum_{s,\bar{s}}\int_0^1 \frac{\mathrm{d}x}{4\pi}\frac{x}{(1-x)^2}\left|\tilde{\psi}_{s\bar{s}}\left(\frac{-\vec{b}_\perp}{1-x},x\right)\right|^2 + \sum_{s,\bar{s}}\int_0^1 \frac{\mathrm{d}x}{4\pi}\frac{1-x}{x^2}\left|\tilde{\psi}_{s\bar{s}}\left(\frac{\vec{b}_\perp}{x},x\right)\right|^2. \tag{13}$$

Each density is normalized to unity, as the unit charge and the total longitudinal momentum of the meson, respectively. The momentum density is more concentrated in the center than the charge density, where the difference is a relativistic effect [12]. This pattern can be observed in Fig. 5, where we present the results of pseudoscalar and scalar states. We compare the rms radii of $\rho_g(\vec{b}_\perp)$ among heavy meson systems, which are 0.84, 0.58, and 0.57 GeV^{-1} for J/Ψ, $B_c(1^3S_1)$, and Υ, respectively. This result is consistent with the trend of decay constants: for the heavier system, it has smaller radii, and therefore it is easier for it to decay.

E. Distribution amplitude

Distribution amplitudes (DAs) are defined from the lightlike vacuum-to-meson matrix elements and can be written with LFWFs as

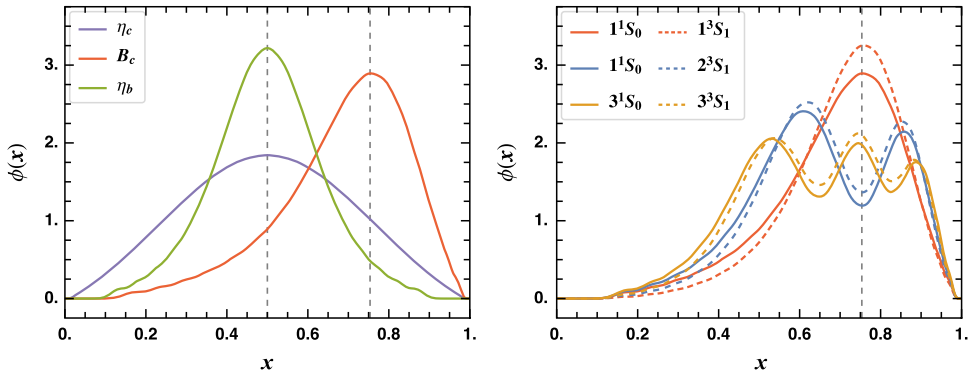

FIG. 6. The DAs of the ground states of charmonium, B_c, and bottomonium (left panel). DAs of the pseudoscalar and vector B_c's and their radial excitations (right panel). Vertical dashed lines indicate the constituent quark mass fraction of the corresponding system. Specifically, peaks of the DAs of quarkonium occur at $x = m_c/(m_c + m_{\bar{c}}) = m_b/(m_b + m_{\bar{b}}) = 1/2$, and the peak of B_c is close to $x = m_b/(m_b + m_{\bar{c}}) \approx 0.75$.

$$\frac{f_{P,V}}{2\sqrt{2N_c}}\phi_{P,V}(x) = \frac{1}{\sqrt{x(1-x)}}\int \frac{d^2\vec{k}_\perp}{2(2\pi)^3}\psi^{\lambda=0}_{\uparrow\downarrow\mp\downarrow\uparrow}(\vec{k}_\perp, x), \tag{14}$$

with $f_{P,V}$ the decay constants for pseudoscalars and vectors, respectively. Note that DAs defined here are normalized to unity. We compare the ground states pseudoscalar DAs of the charmonium, B_c meson, and bottomonium in Fig. 6. The width of the DA decreases, while the peak height increases with the mass of the system, and approaches a δ function in the nonrelativistic limit. For charmonium and bottomonium, peaks are at $x = 1/2$ due to the equal mass of the constituent quark and antiquark, while for B_c, the peak is close to the constituent quark mass fraction, i.e., $x = m_b/(m_b + m_{\bar{c}}) \approx 0.75$, which is consistent with the distribution of the LFWFs in the previous section. We present the DAs of the ground-state pseudoscalar, vector and of their excitations. Note that the pseudoscalar and vector DAs have similar patterns but they are not identical. This is due to the different configuration mixings as controlled by the one-gluon-exchange interaction in this model. The radial excited states have important distinctions: dips appear with the radial excitations. This pattern also appears in charmonium and bottomonium in BLFQ and in other methods [33,34]. Wiggles near both extremes of x arise from the limited range of basis spaces employed.

IV. SUMMARY

In this work, we investigated the unequal-mass meson system $B_c(b\bar{c})$ within the BLFQ approach. All model parameters are fixed by reference to charmonium and bottomonium systems. We found reasonable agreement with existing experiments and with other theoretical calculations.

We carried out the calculations with the basis limit $N_{\max} = L_{\max} = 32$, which corresponds to the specific UV (IR) regulator $b\sqrt{N_{\max}} \approx 6.77\,\mathrm{GeV}(b/\sqrt{N_{\max}} \simeq 0.21\,\mathrm{GeV})$. We first predicted the B_c mass spectrum and presented the LFWFs of some selected states. These results are obtained from diagonalizing a light-front Hamiltonian based on light-front holography. We discussed a significant difference between the LFWFs of B_c and heavy quarkonium: only the unequal-mass system B_c allows both positive and negative charge parities in the wave functions, due to the absence of charge conjugation symmetry.

We calculated other observables with LFWFs such as the decay constants of pseudoscalar and vector states. For additional applications and tests of our model, we calculated transverse charge and momentum densities.

Our successes here in applications of the model for heavy quarkonium to the unequal-mass heavy meson system provide support for further extensions to lighter systems. One anticipates greater challenges to the model which are likely to require the inclusion of a dynamical gluon in a higher Fock sector. This naturally incorporates self-energy processes and raises challenging issues of renormalization [35,36]. Additional significant physics should also be included such as chiral symmetry breaking, etc.

ACKNOWLEDGMENTS

We wish to thank Shaoyang Jia, Meijian Li, Wenyang Qian, and Anji Yu for valuable discussions. We also thank Dr. Zhigang Wang for clarifying the result from the QCD sum rule [22] that we quote in Table III. P. Maris thanks the Fundação de Amparo à Pesquisa do Estado de São Paulo for support under Grant No. 2017/19371-0. This work was supported in part by the U.S. Department of Energy under Grants No. DE-FG02-87ER40371, No. DE-SC0018223 (SciDAC-4/NUCLEI), No. DE-SC0015376 (DOE Topical Collaboration in Nuclear Theory for Double-Beta Decay and Fundamental Symmetries), and DE-FG02-04ER41302. Computational resources were provided by the National Energy Research Supercomputer Center, which is supported by the Office of Science of the U.S. Department of Energy under Contract No. DE-AC02-05CH11231.

[1] F. Abe *et al.* (CDF Collaboration), Phys. Rev. D **58**, 112004 (1998).
[2] G. Aad *et al.* (ATLAS Collaboration), Phys. Rev. Lett. **113**, 212004 (2014).
[3] J. Koponen, A. C. Zimermmane-Santos, C. T. H. Davies, G. P. Lepage, and A. T. Lytle (HPQCD Collaboration), Phys. Rev. D **96**, 054501 (2017).
[4] B. Colquhoun, C. T. H. Davies, J. Kettle, J. Koponen, A. T. Lytle, R. J. Dowdall, and G. P. Lepage (HPQCD Collaboration), Phys. Rev. D **91**, 114509 (2015).
[5] A. Ali, L. Maiani, A. D. Polosa, and V. Riquer, Phys. Rev. D **94**, 034036 (2016).
[6] B. Bhattacharya and A. A. Petrov, Phys. Lett. B **774**, 430 (2017).
[7] B. Bakker, A. Bassetto, S. Brodsky, W. Broniowski, S. Dalley, T. Frederico, S. Głazek, J. Hiller, C.-R. Ji, V. Karmanov, D. Kulshreshtha, J.-F. Mathiot, W. Melnitchouk, G. Miller, J. Papavassiliou, W. Polyzou, N. Stefanis, J. Vary, A. Ilderton, and T. Heinzl, Nucl. Phys. B, Proc. Suppl. **251–252**, 165 (2014).

[8] S. J. Brodsky, G. F. de Téramond, H. G. Dosch, and J. Erlich, Phys. Rep. **584**, 1 (2015).
[9] P. Maris, P. Wiecki, Y. Li, X. Zhao, and J. P. Vary, Acta Phys. Pol. B Proc. Suppl. **6**, 321 (2013).
[10] P. Wiecki, Y. Li, X. Zhao, P. Maris, and J. P. Vary, Phys. Rev. D **91**, 105009 (2015).
[11] Y. Li, P. Maris, X. Zhao, and J. P. Vary, Phys. Lett. B **758**, 118 (2016).
[12] Y. Li, P. Maris, and J. P. Vary, Phys. Rev. D **96**, 016022 (2017).
[13] G. F. de Téramond and S. J. Brodsky, Phys. Rev. Lett. **102**, 081601 (2009).
[14] J. P. Vary, H. Honkanen, J. Li, P. Maris, S. J. Brodsky, A. Harindranath, G. F. de Teramond, P. Sternberg, E. G. Ng, and C. Yang, Phys. Rev. C **81**, 035205 (2010).
[15] H. G. Dosch, G. F. de Téramond, and S. J. Brodsky, Phys. Rev. D **95**, 034016 (2017).
[16] C. Patrignani (Particle Data Group), Chin. Phys. C **40**, 100001 (2016).
[17] I. F. Allison, C. T. H. Davies, A. Gray, A. S. Kronfeld, P. B. Mackenzie, and J. N. Simone (HPQCD, Fermilab Lattice, and UKQCD Collaborations), Phys. Rev. Lett. **94**, 172001 (2005).
[18] E. B. Gregory, C. T. H. Davies, E. Follana, E. Gamiz, I. D. Kendall, G. P. Lepage, H. Na, J. Shigemitsu, and K. Y. Wong (HPQCD Collaboration), Phys. Rev. Lett. **104**, 022001 (2010).
[19] C. Davies, K. Hornbostel, G. Lepage, A. Lidsey, J. Shigemitsu, and J. Sloan, Phys. Lett. B **382**, 131 (1996).
[20] M. Li, Y. Li, P. Maris, and J. P. Vary, Phys. Rev. D **98**, 034024 (2018).
[21] M. J. Baker, J. Bordes, C. A. Dominguez, J. Peñarrocha, and K. Schilcher, J. High Energy Phys. 07 (2014) 032.
[22] Z.-G. Wang, Eur. Phys. J. A **49**, 131 (2013).
[23] H.-M. Choi and C.-R. Ji, Phys. Rev. D **80**, 054016 (2009).
[24] C. T. Tran, M. A. Ivanov, J. G. Körner, and P. Santorelli, Phys. Rev. D **97**, 054014 (2018).
[25] T. Branz, A. Faessler, T. Gutsche, M. A. Ivanov, J. G. Körner, and V. E. Lyubovitskij, Phys. Rev. D **81**, 034010 (2010).
[26] A. A. El-Hady, M. A. K. Lodhi, and J. P. Vary, Phys. Rev. D **59**, 094001 (1999).
[27] R. Benbrik and C.-H. Chen,Phys. Lett. B **672**, 172 (2009).
[28] T. Aliev (private communication).
[29] T. M. Aliev and O. Yilmaz, Nuovo Cimento A **105**, 827 (1992).
[30] M. Burkardt, Int. J. Mod. Phys. A **18**, 173 (2003).
[31] G. A. Miller, Phys. Rev. Lett. **99**, 112001 (2007).
[32] Z. Abidin and C. E. Carlson, Phys. Rev. D **78**, 071502 (2008).
[33] V. V. Braguta, Phys. Rev. D **77**, 034026 (2008).
[34] C.-W. Hwang, Eur. Phys. J. C **62**, 499 (2009).
[35] V. A. Karmanov, J.-F. Mathiot, and A. V. Smirnov, Phys. Rev. D **77**, 085028 (2008).
[36] M. Gómez-Rocha and S. D. Głazek, Phys. Rev. D **92**, 065005 (2015).